Single qubit decoherence under a separable coupling to a random matrix environment

M. Carrera,[1,2] T. Gorin,[3] and T. H. Seligman[2,4]

[1] *Facultad de Ciencias, Universidad Autónoma del Estado de Morelos, Avenida Universidad 1001, C.P. 62209, Cuernavaca, Morelos, México.*
[2] *Instituto de Ciencias Físicas, Universidad Nacional Autónoma de México, Avenida Universidad s/n, 62210 Cuernavaca, Morelos, México.*
[3] *Departamento de Física, Universidad de Guadalajara, Blvd. Marcelino García Barragan y Calzada Olímpica, C.P. 44840, Guadalajara, Jalísco, México.*
[4] *Centro Internacional de Ciencias A.C., Avenida Universidad s/n, 62131 Cuernavaca, Morelos, México.*

arXiv:1405.4448v1 [quant-ph] 18 May 2014

This paper describes the dynamics of a quantum two-level system (qubit) under the influence of an environment modeled by an ensemble of random matrices. In distinction to earlier work, we consider here separable couplings and focus on a regime where the decoherence time is of the same order of magnitude than the environmental Heisenberg time. We derive an analytical expression in the linear response approximation, and study its accuracy by comparison with numerical simulations. We discuss a series of unusual properties, such as purity oscillations, strong signatures of spectral correlations (in the environment Hamiltonian), memory effects and symmetry breaking equilibrium states.

PACS numbers: 03.65.Yz,05.45.Mt,42.50.Lc
Keywords: open quantum systems, random matrix theory, decoherence, memory effects

I. INTRODUCTION

The general idea of random matrix environments consists in formulating the dynamics of an open quantum system (henceforth called the "central system") in terms of the reduced dynamics of a Hamiltonian system which consists of central system and environment. The intention is to use techniques from random matrix theory (RMT) to integrate out the dynamics in the environment, such that from a computational point of view, one only needs to deal with the degrees of freedom of the central system. Since their introduction in Ref. [1], such RMT formulations have received more and more attention. As a result, a variety of different models have been proposed. Some studies have been concentrating on the strong coupling regime [2–4]. A generic RMT coupling with finite coupling strength was discussed in [5]. In all these cases decoherence has been discussed principally in terms of the mean purity, averaged over the RMT ensemble. Instead, in [6] and [7] the average density matrix was calculated. Somewhat different models based on random matrices are given in [8–12]

In the present paper we wish to present a more detailed discussion, expanding the coupling into separable terms, of which, up to now only the dephasing term has been considered explicitly. Only in this case, the problem can be reduced to a fidelity problem in the near environment [13, 14]. Our RMT model may be compared to the master equation for resonance fluorescence [15], or to the Jaynes-Cummings model [16], where a two-level system is coupled to a single harmonic oscillator mode. When compared to the first, the important difference lies in the fact that we have a finite level spacing and assume the decoherence time to be of the order of the environmental Heisenberg time. When compared to the second, the difference is, that we assume a complicated many-body environment about which we know little, essentially with properties similar to those assumed for the nucleus by Wigner [17]. In this spirit the random matrix environment can be considered as the representation of maximal ignorance about this environment [18]. Alternatively, we may consider the RMT environment as a model for a chaotic system as considered in [19, 20], which happens to serve as the environment for a two level system. Interestingly, Ref. [21] reports the experimental realization of a possibly suitable quantum chaotic system.

Our model with separable but otherwise random coupling shows strikingly different and unusual phenomena, depending on the term we use: (i) It can show a strong sensitivity to spectral correlations, which according to the quantum chaos hypothesis [19, 20, 22] may allow to distinguish chaotic and integrable environments, on the basis of the decoherence process. (ii) In spite of the fact that our model defines a unital quantum map [23] for the qubit, it may lead to purity oscillations. (iii) Our model shows an intriguing case of symmetry breaking by the stationary states, as well as memory effects. Some of these properties may be related to different signatures of quantum non-Markovianity, introduced recently [4, 24, 25].

The paper is organized as follows: In Sec. II we introduce our model of an RMT environment with separable coupling, apply the linear response approximation and perform the averages over the random matrices. Sec. III specializes the model to the case of a single qubit as the central system. In Sec. IV we present our numerical simulations, the comparison with the linear response approximation, and discuss the very particular features for different separable couplings. In Sec. V we present our conclusions. Various integrals related to the ensemble averages within the linear response approximation are calculated in the appendix.

II. GENERAL MODEL

The full Hilbert space $\mathcal{H}_\mathrm{c} \otimes \mathcal{H}_\mathrm{e}$ is divided into the Hilbert space of the central system $\mathcal{H}_\mathrm{c}$ and that of the environment $\mathcal{H}_\mathrm{e}$. We assume that the dynamics in the whole Hilbert space is unitary, governed by the Hamiltonian

$$H_\lambda = H_0 + \lambda V \ , \qquad H_0 = H_\mathrm{c} \otimes \mathbb{1} + \mathbb{1} \otimes H_\mathrm{e} \ , \qquad (1)$$

where the real and non negative parameter λ denotes the strength of the coupling between the central system H_c and the environment H_e. For definiteness, we assume H_0 and λ to have units of energy, while the perturbation V itself is dimensionless. We measure time t_ph in units of $\hbar/d_0 = 2\pi\, t_\mathrm{H}$ where t_H is the Heisenberg time of the environment and d_0 is the average level spacing in the spectrum of H_e. In terms of the dimensionless time $t = t_\mathrm{ph} d_0/\hbar$, the evolution operator may be written as $U(t) = \exp[-\mathrm{i}H_\lambda t/d_0]$. In order to complete the change to dimensionless quantities, we choose $\lambda = d_0\,\mu$, $H_\mathrm{c} = d_0\, h_\mathrm{c}$ and $H_\mathrm{e} = d_0\, h_\mathrm{e}$ such that

$$H_\lambda = d_0\, h_\mu \ , \qquad h_\mu = h_0 + \mu\, V \ . \qquad (2)$$

Hence, $U(t) = \exp[-\mathrm{i}h_\mu\, t]$, and $h_0 = h_\mathrm{c} \otimes \mathbb{1} + \mathbb{1} \otimes h_\mathrm{e}$. In contrast to earlier work [5, 6], the coupling operator V is now assumed to be separable:

$$V = v_\mathrm{c} \otimes V_\mathrm{e} \ , \qquad (3)$$

where V_e is a random matrix chosen from one of the Gaussian invariant ensembles [26]. In what follows, we may want to distinguish the case where v_c commutes with h_c (dephasing coupling [13, 14]) and the case where it does not commute.

At a first stage, we follow [6] in order to calculate the density matrix of the central system

$$\varrho_\mathrm{c}(t) = \mathrm{tr}_\mathrm{e}\left[\mathrm{e}^{-\mathrm{i}h_\mu t}\, \varrho_0\, \mathrm{e}^{\mathrm{i}h_\mu t}\right] \ , \quad \varrho_0 = \varrho_\mathrm{c} \otimes \varrho_\mathrm{e} \ . \qquad (4)$$

This yields still without any approximation (for details see Sec. 2 of [6])

$$\varrho_\mathrm{c}(t) = u_\mathrm{c}\ \tilde{\varrho}_\mathrm{c}(t)\ u_\mathrm{c}^\dagger \ , \qquad \tilde{\varrho}_\mathrm{c}(t) = \mathrm{tr}_\mathrm{e}\big[\,\varrho_M(t)\,\big] \ , \qquad (5)$$

where $\varrho_M(t)$ stands for the density operator in the interaction picture:

$$\varrho_M(t) = M_\mu(t)\ \varrho_0\ M_\mu(t)^\dagger \ , \quad M_\mu(t) = \mathrm{e}^{\mathrm{i}h_0\, t}\ \mathrm{e}^{-\mathrm{i}h_\mu\, t} \ . \qquad (6)$$

In the following sections, we introduce the linear response approximation, where we will be able to perform the averages over the random matrices in $\varrho_M(t)$.

A. Linear response approximation

In order to apply linear response theory, we develop $M_\mu(t)$ into its Dyson series, and consider terms up to second order in μ. This yields

$$\tilde{\varrho}_\mathrm{c}(t) = \varrho_\mathrm{c} - \mu^2\, \mathrm{tr}_\mathrm{e}\big[\, J(t)\,\varrho_0 + \varrho_0\, J(t)^\dagger + I(t)\,\varrho_0\, I(t)\,\big] \ , \qquad (7)$$

where

$$I(t) = \int_0^t \mathrm{d}s\ \tilde{V}(s) \ , \quad J(t) = \int_0^t \mathrm{d}s \int_0^s \mathrm{d}s'\ \tilde{V}(s)\,\tilde{V}(s') \ . \qquad (8)$$

Due to the separability of V, we find for its representation in the interaction picture

$$\begin{aligned}\tilde{V}(t) &= \mathrm{e}^{\mathrm{i}\,h_\mathrm{c}\,t} \otimes \mathrm{e}^{\mathrm{i}\,h_\mathrm{e}\,t}\ v_\mathrm{c} \otimes V_\mathrm{e}\ \mathrm{e}^{-\mathrm{i}\,h_\mathrm{c}\,t} \otimes \mathrm{e}^{-\mathrm{i}\,h_\mathrm{e}\,t} \\ &= u_\mathrm{c}^\dagger\ v_\mathrm{c}\ u_\mathrm{c} \otimes u_\mathrm{e}^\dagger\ V_\mathrm{e}\ u_\mathrm{e} = \tilde{v}_c(t)\ \otimes\ \tilde{V}_\mathrm{e}(t) \ . \end{aligned} \qquad (9)$$

B. Random matrix averages

Our model contains two random matrices, the coupling matrix V_e (with matrix elements V_{jl}) and the environment Hamiltonian h_e. In this section we consider the case where V_e is chosen from the Gaussian unitary ensemble (GUE) and the Gaussian orthogonal ensemble (GOE), while for h_e, we only assume that it can be diagonalized leaving the respective ensemble invariant. Under such conditions we can arrive at a very compact expression for the average reduced state $\langle\varrho_\mathrm{c}(t)\rangle$. Note however that later on we will restrict ourselves to the GUE.

To obtain the ensemble average of the reduced state $\langle\varrho_\mathrm{c}(t)\rangle$, we first perform the average over V_e and later that over h_e. In view of Eq. (7), we divide that calculation in two parts, the calculation of $\langle J(t)\rangle$ and $\langle I(t)\,\varrho_0\, I(t)\rangle$, respectively.

$$\begin{aligned}\langle J(t)\rangle &= \int_0^t \mathrm{d}s \int_0^s \mathrm{d}s'\ \tilde{v}_c(s)\tilde{v}_c(s') \\ &\quad \otimes \left\langle \sum_{jln} |j\rangle\ \mathrm{e}^{\mathrm{i}(E_j - E_l)s}\ V_{jl}\ \mathrm{e}^{\mathrm{i}(E_l - E_n)s'}\ V_{ln}\ \langle n| \right\rangle \\ &= \int_0^t \mathrm{d}s \int_0^s \mathrm{d}s'\ \tilde{v}_c(s)\ \tilde{v}_c(s') \\ &\quad \otimes \sum_{jln} |j\rangle\ \mathrm{e}^{\mathrm{i}(E_j - E_l)s}\ \delta_{jn}\ \mathrm{e}^{\mathrm{i}(E_l - E_n)s'}\ \langle n| \ . \end{aligned} \qquad (10)$$

The term $\delta_{jl}\delta_{ln} = \delta_{jn}\delta_{ln}$ is present in the GOE case ($\beta = 1$), but absent in the GUE case ($\beta = 2$). Therefore,

$$\begin{aligned}\langle J(t)\rangle &= \int_0^t \mathrm{d}s \int_0^s \mathrm{d}s'\ \tilde{v}_c(s)\tilde{v}_c(s') \\ &\quad \otimes \sum_n |n\rangle\langle n| \left(3 - \beta + \textstyle\sum_{l\neq n} \mathrm{e}^{\mathrm{i}(E_n - E_l)(s-s')}\right) \\ &= \int_0^t \mathrm{d}s \int_0^s \mathrm{d}s'\ c(s-s')\ \tilde{v}_c(s)\tilde{v}_c(s') \otimes \mathbb{1} \ , \end{aligned} \qquad (11)$$

where β is the so called Dyson parameter, and

$$c(t) = 3 - \beta + \delta\left(\frac{t}{2\pi}\right) - b_2\left(\frac{t}{2\pi}\right) \ . \qquad (12)$$

The calculation presented here is completely analogous to the one in Ref. [27], where we worked out the linear response result for fidelity decay in a similar RMT

model. The function $b_2(t)$ is the so called two-point form factor [26]. For the average over the second term we find

$$\langle I(t)\,\varrho_0\,I(t)\rangle = \int_0^t \mathrm{d}s \int_0^t \mathrm{d}s'\;\tilde{v}(s)\;\varrho_\mathrm{c}\;\tilde{v}(s') \sum_{jln} \mathrm{e}^{\mathrm{i}E_j(s-s')} \times\; (\delta_{ln}+\delta_{jn}\delta_{lj})\;\mathrm{e}^{-\mathrm{i}(E_l s - E_n s')}\;\varrho^\mathrm{e}_{ln}\;, \tag{13}$$

where we have used that ϱ_0 is separable: $\varrho_0 = \varrho_\mathrm{c}\otimes\varrho_\mathrm{e}$. Since $\delta_{ln}+\delta_{jn}\delta_{lj} = \delta_{ln}(1+\delta_{jn})$, we obtain

$$\langle I(t)\,\varrho_0\,I(t)\rangle = \int_0^t \mathrm{d}s \int_0^t \mathrm{d}s'\;\tilde{v}(s)\;\varrho_\mathrm{c}\;\tilde{v}(s') \times \sum_{jn} \mathrm{e}^{\mathrm{i}(E_j-E_n)(s-s')}\;(1+\delta_{jn})\;\varrho^\mathrm{e}_{nn} \tag{14}$$

in the GOE case, and

$$\begin{aligned}\langle I(t)\,\varrho_0\,I(t)\rangle &= \int_0^t \mathrm{d}s \int_0^t \mathrm{d}s'\;\tilde{v}(s)\;\varrho_\mathrm{c}\;\tilde{v}(s') \times \left[3-\beta+\textstyle\sum_n \varrho^\mathrm{e}_{nn}\sum_{j\neq n}\mathrm{e}^{\mathrm{i}(E_j-E_n)(s-s')}\right] \\ &= \int_0^t \mathrm{d}s \int_0^t \mathrm{d}s'\;c(s-s')\;\tilde{v}(s)\;\varrho_\mathrm{c}\;\tilde{v}(s')\;. \end{aligned} \tag{15}$$

in general. With both results, we obtain:

$$\begin{aligned}\tilde{\varrho}_\mathrm{c}(t) &= \varrho_\mathrm{c} \\ &- \mu^2 \int_0^t \mathrm{d}s \int_0^s \mathrm{d}s'\;c(s-s')\;\big[\,\tilde{v}_c(s)\,,\,[\tilde{v}_c(s'),\varrho_c]\,\big]\;. \end{aligned} \tag{16}$$

III. SINGLE QUBIT CENTRAL SYSTEM

For a general two level system as central system, we may assume without restriction that h_c is given by

$$h_\mathrm{c} = \frac{\Delta}{2}\;\sigma_z\;, \tag{17}$$

with Δ being the energy difference between the two eigen states of the qubit, measured in units of the mean level spacing d_0 in the environment; cf. Eq. (2). The matrix σ_z is one of the three Pauli matrices [23]

$$\sigma_x = \begin{pmatrix}0 & 1\\ 1 & 0\end{pmatrix}\;,\quad \sigma_y = \begin{pmatrix}0 & -\mathrm{i}\\ \mathrm{i} & 0\end{pmatrix}\;,\quad \sigma_z = \begin{pmatrix}1 & 0\\ 0 & -1\end{pmatrix}\;. \tag{18}$$

We consider the single qubit coupled to a large environment via a separable coupling, where the qubit-part of the coupling either commutes with the system part ($v_\mathrm{c}=\sigma_z$) or not. The former case is called "dephasing coupling" [13, 14], while in the latter case, we choose $v_\mathrm{c}=\sigma_x$ (this is equivalent to any linear combination of σ_x and σ_y). Note that we can obtain the general RMT Hamiltonian for the central system as a random linear combination of these terms.

A. Dephasing coupling, $v_\mathrm{c} = \sigma_z$

In this case, the evolution in the environment only depends parametrically on the state of the central system (dephasing situation) [13, 14]. That allows one to find an exact analytical expression for the RMT average of the reduced dynamics in terms of fidelity decay [28, 29]. In this section, we nevertheless use the linear response approximation. This allows us to make contact with fidelity calculation in Ref. [27], and it serves us as a test case, before embarking on the case $v_\mathrm{c}=\sigma_x$, which is at the center of our interest.

For $v_\mathrm{c}=\sigma_z$, we find for the coupling operator in the interaction picture:

$$v_\mathrm{c} = \begin{pmatrix}1 & 0\\ 0 & -1\end{pmatrix}\;,\quad \tilde{v}_\mathrm{c}(s) = \tilde{v}_\mathrm{c}(s') = \begin{pmatrix}1 & 0\\ 0 & -1\end{pmatrix}\;. \tag{19}$$

In order to evaluate the linear response expression in Eq. (16), we need the commutators

$$\begin{aligned}[\tilde{v}_\mathrm{c}(s')\,,\,\varrho_\mathrm{c}] &= \begin{pmatrix}1 & 0\\ 0 & -1\end{pmatrix}\begin{pmatrix}a & b^*\\ b & c\end{pmatrix} - \begin{pmatrix}a & b^*\\ b & c\end{pmatrix}\begin{pmatrix}1 & 0\\ 0 & -1\end{pmatrix} \\ &= \begin{pmatrix}0 & 2b^*\\ -2b & 0\end{pmatrix}\;, \end{aligned} \tag{20}$$

and

$$\begin{aligned}[\tilde{v}_\mathrm{c}(s)\,,\,\ldots] &= \begin{pmatrix}1 & 0\\ 0 & -1\end{pmatrix}\begin{pmatrix}0 & 2b^*\\ -2b & 0\end{pmatrix} \\ &\quad - \begin{pmatrix}0 & 2b^*\\ -2b & 0\end{pmatrix}\begin{pmatrix}1 & 0\\ 0 & -1\end{pmatrix} = \begin{pmatrix}0 & 4b^*\\ 4b & 0\end{pmatrix}\;, \end{aligned} \tag{21}$$

where we introduced the notation "..." on the left side to denote $[\tilde{v}_\mathrm{c}(s')\,,\,\varrho_\mathrm{c}]$. As expected in this "dephasing" case, only the off-diagonal elements of the central system's density matrix are affected.

If the initial state is an eigenstate of σ_z, then there is no evolution at all. On the other hand, for a pure state in the (x,y)-plane of the Bloch sphere (for the sake of definiteness, we choose the symmetric eigenstate of σ_x), we obtain

$$|\psi\rangle = \frac{1}{\sqrt{2}}\,\big(\,|0\rangle+|1\rangle\,\big)\;,\quad \varrho_\mathrm{c} = |\psi\rangle\langle\psi| = \frac{1}{2}\begin{pmatrix}1 & 1\\ 1 & 1\end{pmatrix}\;, \tag{22}$$

such that $a=b=c=1/2$. Therefore:

$$\begin{aligned}\langle\tilde{\varrho}_\mathrm{c}^{21}(t)\rangle &= \frac{1}{2} - \mu^2\int_0^t \mathrm{d}s\int_0^s \mathrm{d}s'\;c(s-s')\;2 \\ &= \frac{1}{2}\left[1-4\mu^2\;C_\mathrm{fid}(t)\right]\;. \end{aligned} \tag{23}$$

The function $C_\mathrm{fid}(t)$ is evaluated in App. 1 with the result:

$$C_\mathrm{fid}(t) = \begin{cases}\pi t + t^3/(12\pi) & : t<2\pi\;,\\ t^2/2 + 2\pi^2/3 & : t>2\pi\;,\end{cases} \tag{24}$$

in agreement with the general result in Ref. [27].

B. Non-commuting coupling, $v_c = \sigma_x$

In general, the coupling operator v_c may be written as a linear combination of the Pauli matrices, defined in Eq. (18). Since we have analyzed the case, where v_c commutes with the system Hamiltonian, we are now looking for cases where v_c does not commute. In fact, we would like to avoid that the coupling operators has any commuting component. This restricts v_c to a linear combination of σ_x and σ_y. Since the only other non-trivial central system operator in the Hamiltonian is σ_z, we may choose $v_c = \sigma_x$ without restricting generality. Hence, the dynamics in our model only depends on the initial state ϱ_c of the qubit, i.e. its orientation in the Bloch sphere, with respect to the system Hamiltonian σ_z and the coupling operator σ_x. The linear response calculation then gives:

$$\tilde{v}_c(s') = \begin{pmatrix} e^{i\Delta s'/2} & 0 \\ 0 & e^{-i\Delta s'/2} \end{pmatrix} \begin{pmatrix} 0 & 1 \\ 1 & 0 \end{pmatrix} \begin{pmatrix} e^{-i\Delta s'/2} & 0 \\ 0 & e^{i\Delta s'/2} \end{pmatrix} , \tag{25}$$

which results in

$$\tilde{v}_c(s') = \begin{pmatrix} 0 & \kappa_1 \\ \kappa_1^* & 0 \end{pmatrix} , \quad \tilde{v}_c(s) = \begin{pmatrix} 0 & \kappa_2 \\ \kappa_2^* & 0 \end{pmatrix} , \tag{26}$$

where $\kappa_1 = e^{i\Delta s'}$, and $\kappa_2 = e^{i\Delta s}$. For the commutators we then obtain:

$$\begin{aligned} [\tilde{v}_c(s')\,,\,\varrho_c] &= \begin{pmatrix} \kappa_1 b - \kappa_1^* b^* & -\kappa_1(a-c) \\ \kappa_1^*(a-c) & -(\kappa_1 b - \kappa_1^* b^*) \end{pmatrix} \\ &= \begin{pmatrix} Q & -\kappa_1 R \\ \kappa_1^* R & -Q \end{pmatrix} , \end{aligned} \tag{27}$$

where $Q = \kappa_1 b - \kappa_1^* b^*$ and $R = a - c$. Finally:

$$\begin{aligned} [\tilde{v}_c(s)\,,\,\ldots] &= \begin{pmatrix} 0 & \kappa_2 \\ \kappa_2^* & 0 \end{pmatrix} \begin{pmatrix} Q & -\kappa_1 R \\ \kappa_1^* R & -Q \end{pmatrix} \\ &\quad - \begin{pmatrix} Q & -\kappa_1 R \\ \kappa_1^* R & -Q \end{pmatrix} \begin{pmatrix} 0 & \kappa_2 \\ \kappa_2^* & 0 \end{pmatrix} \\ &= \begin{pmatrix} (\kappa_1\kappa_2^* + \kappa_1^*\kappa_2)\, R & -2\kappa_2\, Q \\ 2\kappa_2^*\, Q & -(\kappa_1\kappa_2^* + \kappa_1^*\kappa_2)\, R \end{pmatrix} . \end{aligned} \tag{28}$$

In what follows, we derive explicit expressions for the matrix elements of the reduced quantum state, for different initial states, first for eigenstates of σ_x (the coupling operator), then for eigenstates of σ_y, and finally for eigenstates of σ_z (the central system operator).

1. Eigenstates of the coupling operator σ_x

For definiteness, we consider the initial state ϱ_c to be the eigenstate of σ_x with eigenvalue $+1$. This implies that $a = b = c = 1/2$, $Q = (\kappa_1 - \kappa_1^*)/2 = i\,\sin(\Delta s')$ and $R = 0$. Therefore, Eq. (28) yields

$$[\tilde{v}_c(s)\,,\,\ldots] = 2i\,\sin(\Delta s') \begin{pmatrix} 0 & -e^{i\Delta s} \\ e^{-i\Delta s} & 0 \end{pmatrix} . \tag{29}$$

Thus, in the present case, we have again a dephasing situation. While the diagonal elements of the average density matrix remain constant, the off-diagonal element becomes

$$\begin{aligned} \langle\tilde{\varrho}_c^{21}(t)\rangle &= \frac{1}{2} - 2i\,\mu^2 \int_0^t ds\, e^{-i\Delta s} \int_0^s ds'\, c(s-s')\, \sin(\Delta s') \\ &= \frac{1}{2}\big[\,1 - 4\,\mu^2\, C_x(t)\,\big] , \end{aligned} \tag{30}$$

with the change of variable $s' \to u = s - s'$ the function $C_x(t)$ becomes

$$C_x(t) = i \int_0^t du\, c(u) \int_u^t ds\, e^{-i\Delta s}\, \sin\left[\Delta(s-u)\right] \tag{31}$$

is again evaluated in App. with the result given in the Eqs. (A.6) and (A.7).

2. Eigenstates of σ_y

We choose the eigenstate $|\psi\rangle = (|0\rangle + i\,|1\rangle)/\sqrt{2}$ which has eigenvalue $+1$. Then

$$\varrho_c = \frac{1}{2} \begin{pmatrix} 1 & -i \\ i & 1 \end{pmatrix} \tag{32}$$

such that $Q = i\,(\kappa_1 + \kappa_1^*)/2$ and $R = 0$. Hence

$$\begin{aligned} [\tilde{v}_c(\sigma)\,,\,\ldots] &= \begin{pmatrix} 0 & -i\,\kappa_2\,(\kappa_1 + \kappa_1^*) \\ i\,\kappa_2^*\,(\kappa_1 + \kappa_1^*) & 0 \end{pmatrix} \\ &= 2i\,\cos(\Delta s') \begin{pmatrix} 0 & -e^{i\Delta s} \\ e^{-i\Delta s} & 0 \end{pmatrix} . \end{aligned} \tag{33}$$

The result is quite similar to the σ_x eigenstate case. The diagonal elements of the average density matrix remain again constant, while the non-diagonal element becomes

$$\langle\tilde{\varrho}_c^{21}(t)\rangle = \frac{i}{2}\big[\,1 - 4\mu^2\, C_y(t)\,\big] , \tag{34}$$

where

$$C_y(t) = \int_0^t du\, c(u) \int_u^t ds\, e^{-i\Delta s}\, \cos[\Delta(s-u)] . \tag{35}$$

The expression for $C_y(t)$ differs from that for $C_x(t)$ in Eq. (31) only in as much as the sine function in Eq. (31) is replaced here by the cosine function. The result of the evaluation of the integrals is given in Eqs. (A.11) and (A.12).

3. Eigenstates of the system Hamiltonian σ_z.

For definiteness, we again choose the eigenstate corresponding to the eigenvalue $+1$. Thus, the initial state is given by the density matrix

$$\varrho_c = |0\rangle\langle 0| , \quad a = 1 , \quad b = c = 0 , \quad Q = 0 , \quad R = 1 . \tag{36}$$

Therefore, we have

$$[\tilde{v}_{\rm c}(s)\,,\,\ldots\,] = 2\,\cos\left[\Delta(s-s')\right]\begin{pmatrix}1 & 0\\ 0 & -1\end{pmatrix}\,. \tag{37}$$

This means that the non-diagonal elements of the average density matrix will remain zero, while

$$\langle\tilde{\varrho}_{\rm c}^{11}(t)\rangle = 1 - 2\mu^2\,C_z(t)\,, \tag{38}$$

in the same way as above, we do a change of variable $s' \to u = s - s'$ which yields

$$C_z(t) = \int_0^t {\rm d}u\; c(u)\;\cos(\Delta\,u)\;(t-u) \tag{39}$$

and $\langle\tilde{\varrho}_{\rm c}^{22}(t)\rangle = 1 - \langle\tilde{\varrho}_{\rm c}^{11}(t)\rangle$. The result of the evaluation of the integral is given in Eqs. (A.13) and (A.16).

IV. NUMERICAL SIMULATIONS

For the simulation of the reduced dynamics defined in Eq. (4), we need the random matrices, $h_{\rm e}$ and $V_{\rm e}$. The matrix $V_{\rm e}$ is a GUE matrix normalized such that the off-diagonal elements have unit variance, while $h_{\rm e}$ is a diagonal matrix of eigenvalues of a GUE, unfolded to unit mean level spacing across the full spectral range. The initial state is a separable pure state, while the environmental part is given by a random state, chosen to be invariant under arbitrary unitary transformations [30]. From a theoretical point of view this choice is entirely equivalent to the initial condition $\varrho_{\rm e} = \mathbb{1}/N_{\rm e}$. However, the evolution of a pure state can be obtained from the solution of the corresponding Schrödinger equation, while a mixed initial state would require to solve a von Neumann equation. The latter is much more time consuming and therefore impractical. Unless stated otherwise, we choose $N_{\rm e} = 200$ for the dimension of the environment, and for every simulation we average over $n_{\rm run} = 300$ realisations.

We consider the reduced dynamics of the qubit in the so called universal regime, where the RMT model is expected to yield similar results as dynamical models, satisfying the quantum chaos conjecture [20]. That means that the time scales considered are of the order of the Heisenberg time (in our units, this is at $t = 2\pi$), more precisely we require $N_{\rm e}^{-1} \ll t/(2\pi) \ll N_{\rm e}$. Due to these restrictions, we choose the coupling strength μ sufficiently weak, such that the decoherence time fulfills the above inequalities. The reduced dynamics of the qubit also depends on the level splitting Δ (in units of d_0). In a standard situation, we expect $1 \ll \Delta \ll N_{\rm e}$, meaning that from the central system point of view, the spectrum of the environment is both, dense and infinitely large. However, we will find interesting effects when Δ is of the order of one or even smaller.

In the dephasing case ($v_{\rm c} = \sigma_z$), the behavior of the qubit state is well understood and its dependence on Δ becomes trivial (cf. Sec. III A). Therefore, we restrict our numerical analysis to the case $v_{\rm c} = \sigma_x$. In what follows, we will discuss the general features of the qubit dynamics (in Sec. IV A), the effect of spectral correlations (in Sec. IV B), the accuracy of the linear response approximation (in Sec. IV C), and finally some non-trivial results for the equilibrium state – i.e. the state reached at $t \to \infty$ (in Sec. IV D).

Decoherence is measured in terms of purity,

$$P(t) = {\rm tr}\big[\,\langle\varrho_{\rm c}(t)\rangle^2\,\big]\,, \tag{40}$$

calculated from the average density matrix of the qubit obtained from averaging over $n_{\rm run}$ realisations of the reduced dynamics defined in Eq. (4).

A. General behavior

In this section, we fix the coupling strength to $\mu = 0.1$ and the level splitting in the qubit Hamiltonian to $\Delta = 1$. Following the classification in echo dynamics [31], $\mu = 0.1$ puts us well into the crossover area between the Fermi golden rule and the perturbative regimes. Also $\Delta = 1$ is an intermediate choice. For $\Delta \gg 1$ we would expect an exponential behavior, similar to open systems described by quantum master equations. By contrast, for $\Delta \ll 1$, it is actually difficult for the central system to couple to the environment, since the level repulsion reduces the probability to find transitions which meet the excitation energy Δ for the qubit.

The following figures show results for the matrix elements of the average density matrix $\langle\varrho_{\rm c}(t)\rangle$ of the qubit, and for the purity $P(t)$, as defined in Eq. (40). As initial states for the qubit, we choose the symmetric eigenstates of the Pauli matrices, *i.e.* those eigenstates which correspond to the eigenvalue $+1$. Thus, we will show three cases, one for each Pauli matrix, given in Eq. (18).

a. Eigenstate of $\boldsymbol{\sigma_x}$ In Fig. 1 we show simulations for the reduced dynamics of the qubit where the initial state is chosen as the symmetric eigenstate of σ_x. The results suggest that the evolving qubit state is of the form

$$\langle\varrho_{\rm c}(t)\rangle = \frac{1}{2}\begin{pmatrix}1 & z^*(t)\\ z(t) & 1\end{pmatrix}\,, \tag{41}$$

which corresponds to a trajectory in the xy plane in the Bloch sphere. For this reason, we only consider the non-diagonal element of the qubit state in panel (a) of Fig. 1. The deviations of the diagonal elements from the value $1/2$ are very small and well within the expected statistical error. The oscillations which can be seen on panel (a), stem from the central system Hamiltonian, which forces the qubit to rotate around the z-axis. On panel (b) we show the purity, which in the present case can be written as

$$P(t) = \frac{1 + |z(t)|^2}{2}\,. \tag{42}$$

We checked that the somewhat irregular oscillations around an apparently exponential decay of $|z(t)|^2$ are

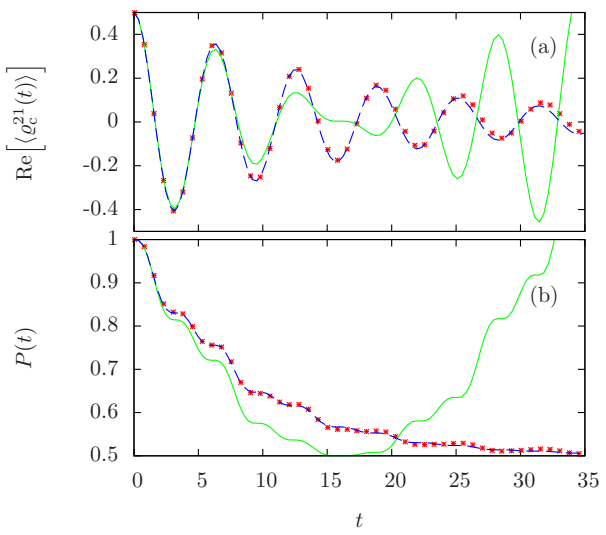

FIG. 1. (Color online) The reduced dynamics for the symmetric eigenstate of σ_x as initial state, for $\Delta = 1$ and $\lambda = 0.1$ as a function of rescaled time t, where the Heisenberg time is $t = 2\pi$. Numerical simulations (red points) are compared to the linear response theory (green solid line) and its exponentiated version (blue dashed line). In panel (a) we show the real part of $\langle\varrho_c^{21}(t)\rangle$, in panel (b) the purity of $\langle\varrho_c(t)\rangle$.

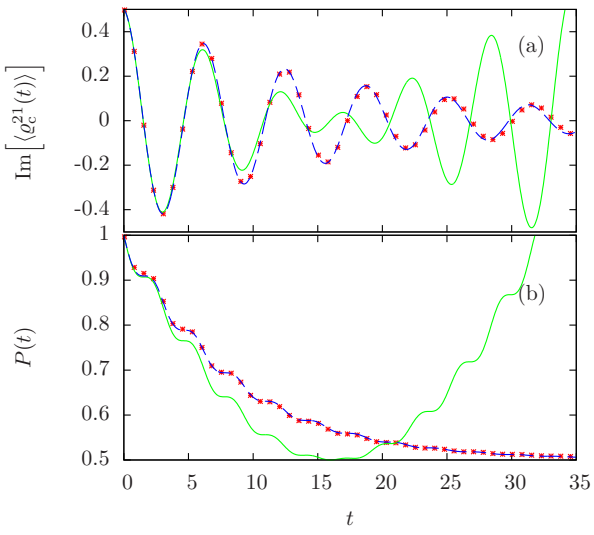

FIG. 2. (Color online) The reduced dynamics for the symmetric eigenstate of σ_y as initial state, for $\Delta = 1$ and $\lambda = 0.1$ as a function of rescaled time, where the Heisenberg time is at $t = 2\pi$. Numerical simulations (red points) are compared to the linear response theory (green solid line) and its exponentiated version (blue dashed line). Panel (a) shows the imaginary part of $\langle\varrho_c^{21}(t)\rangle$, and (b) the purity of $\langle\varrho_c(t)\rangle$.

not of statistical nature. They reflect the dynamics of the true RMT average of the reduced dynamics.

For the present case, the linear response approximation yields the expression given in Eqs. (30) and (31), plotted as a green solid line in Fig. 1. We can see that at least for short times, the approximation describes the true evolution very well. For larger times, we see clear deviations which eventually end up in unphysical behavior. Of course this has to be expected, since the approximation is based on the truncation of a series expansion. Guided by the success of the "exponentiation" of the linear response approximation in the case of fidelity decay [27], we try the same trick here, and apply the following replacement to Eq. (30):

$$1 - 4\mu^2\, C_x(t) \quad \rightarrow \quad \mathrm{e}^{-4\mu^2\, C_x(t)}\,. \tag{43}$$

We refer to this result as the "exponentiated linear response approximation" (ELR for short). It is shown by blue dashed lines in Fig. 1. The agreement with the numerical simulations is greatly improved, in the behavior of the coherence $\langle\varrho_c(t)\rangle$, panel (a), as well as the purity $P(t)$, panel (b). A more detailed analysis of the accuracy of the ELR is provided in Sec. IV C.

b. Eigenstate of $\boldsymbol{\sigma_y}$ The simulations shown in Fig. 2 are entirely analogous to those of Fig. 1, except for the different initial state, which is here a symmetric eigenstate of σ_y. The behavior of the average reduced density matrix is very similar also, and suggests that Eq. (41) and (42) apply as well. Note however, that panel (a) of Fig. 2 shows the imaginary part of $\langle\varrho_c^{21}(t)\rangle$ and that the purity in panel (b) shows a slightly different behavior than in Fig. 1, as can be seen most clearly at very small times. The accuracy of the linear response approximation and its exponentiation is again very similar to the previous case. For the exponentiation we apply the replacement $1 - 4\mu^2\, C_y(t) \rightarrow \exp[-4\mu^2\, C_y(t)]$ to Eq. (34). As can be seen in Fig. 2, the agreement between numerical simulation (red points) and the ELR result (blue dashed line) is surprisingly good.

c. Eigenstate of $\boldsymbol{\sigma_z}$ In Fig. 3, we show simulations for the reduced dynamics of the qubit, where the initial state is chosen as $|1\rangle\langle 1|$, the eigenstate of σ_z corresponding to the eigenvalue $+1$. The results suggest that the evolving qubit state is of the form

$$\langle\varrho_c(t)\rangle = \begin{pmatrix} r(t) & 0 \\ 0 & 1 - r(t) \end{pmatrix}\,, \tag{44}$$

which corresponds to a trajectory restricted to the z-axis in the Bloch sphere. For this reason, we only consider the diagonal element $\langle\varrho_c^{11}(t)\rangle = r(t)$ in panel (a) of Fig. 3. The residual fluctuations of the non-diagonal elements are very small and well within the expected statistical error. For the purity of the average qubit state, we therefore find:

$$P(t) = r(t)^2 + [1 - r(t)]^2 = r^2 + 1 + r^2 - 2r = 1 - 2r(1 - r)\,. \tag{45}$$

Even though Δ and μ have been chosen as in the previous cases, the qubit state does clearly not tend to the maximally mixed state as it seemed to be the case before. For

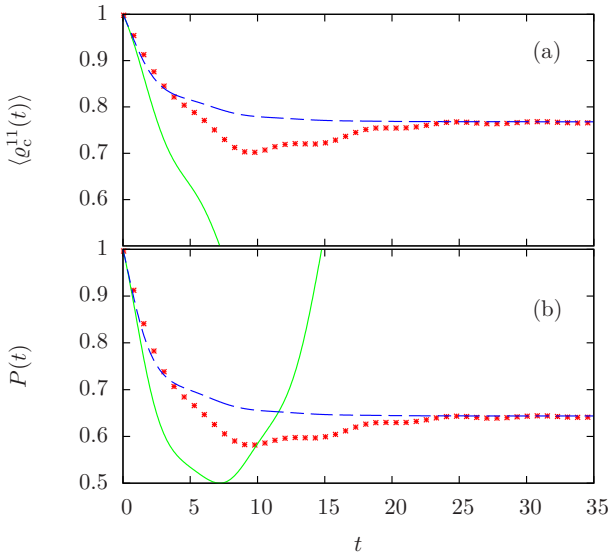

FIG. 3. (Color online) The reduced dynamics of the qubit for the symmetric eigenstate of σ_z as initial state, for $\Delta = 1$ and $\lambda = 0.1$ as a function of rescaled time t, where the Heisenberg time is at $t = 2\pi$. Numerical simulations (red points) are compared to the linear response theory (green solid line) and its exponentiation (blue dashed line). Panel (a) shows the average diagonal element $\langle \varrho_c^{11}(t) \rangle$ and panel (b) the purity of $\langle \varrho_c(t) \rangle$.

large times, we rather end up with a finite polarization: $\lim_{t\to\infty} 2r(t) - 1 \approx 55\%$.

In the present case, the linear response approximation (green solid lines) provides a rather unsatisfying description. The agreement with the numerical simulation is restricted to very small times, and the exponentiation (blue dashed lines) does not really improve the situation. For the exponentiation, we apply the replacement

$$1-2\mu^2\, C_z(t) \to b+(1-b)\, \exp[-2\mu^2/(1-b)\, C_z(t)]\ , \quad (46)$$

to Eq. (38), where the value of b is fitted to the numerical simulation.

B. Effect of spectral correlations

We saw from the linear response calculation, that the dynamics of the qubit is affected by the type of correlations present in the spectrum of the Hamiltonian h_e describing the dynamics in the environment, namely via the two-point form factor introduced in Eq. (12). Quite generally, the effect is such that spectral correlations with positive two-point function, typical for quantum chaotic systems, lead to slower decoherence or fidelity decay than the spectral correlations of typical integrable systems, where the two-point function tends to be zero [22, 32]. For RMT models, this apparently counterintuitive result has been observed already in Ref. [27]. For dynamical

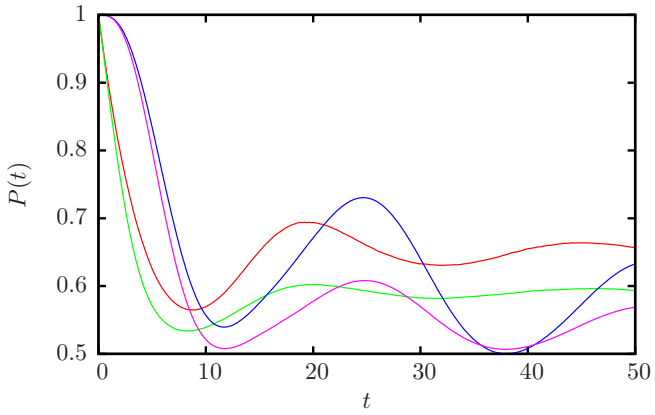

FIG. 4. (Color online) The purity of the average reduced qubit state, as a function of rescaled time t, for spectra with GUE correlations (red and blue lines) and without correlations (green and purple lines). For coupling strength and level splitting, we choose $\mu = 0.1$ and $\Delta = 0.25$. As initial condition, we consider an eigenstate of σ_z (red and green lines) and of σ_x (blue and purple lines).

systems it has been observed even earlier [33, 34] with more dramatic effects and a somewhat different semiclassical explanation.

In our model which is based on unitarily invariant ensembles, only spectral correlations are relevant, so that we expect a possible effect to be largest at times of the order of the Heisenberg time. This implies that the coupling strength should be such that the decoherence time is of that size (cross-over regime). We therefore fix the coupling strength at $\mu = 0.1$. In order to study the effect of interest, we replaced in the diagonal Hamiltonian h_e the unfolded GUE spectrum by independent random numbers, with the same uniform level density. Similar RMT ensembles with uncorrelated levels have been introduced in the context of statistical scattering [35, 36].

Fig. 4 shows the purity $P(t)$ as a function of time, for $\Delta = 0.25$ the initial state being an eigenstate of σ_z (red and green lines) and σ_x (blue and purple lines). In both cases, the replacement of the GUE eigenvalues with uncorrelated random levels results in a very clear additional loss of purity. The effect is clearest at times of the order of 4 times the Heisenberg time ($t \approx 25$), which is reasonable in view of the fact that then the resonance condition $\Delta t \approx 2\pi$ is fulfilled. Note that the central system can couple particularly efficiently to the environment, when the level splitting in the central system is in resonance with the transition between two levels in the environment. Comparing the level spacing distributions for GUE spectra (Wigner surmise) and uncorrelated spectra (Poisson statistics) [22, 26], we see that the probability to find levels with a distance $\Delta = 0.25$ is much more likely in the latter case. By consequence uncorrelated spectra lead to more pronounced decoherence.

We also performed simulations with $\Delta = 1$. However, in this case the difference in decoherence between GUE

and uncorrelated spectra was much smaller. This confirms our explanation, since the probability to find levels with distances close to one, is very similar whether the spectrum shows level repulsion or not.

C. Accuracy of the linear response approximation

In Ref. [27] it was shown that the exponentiation of the linear response result yields a uniform approximation, providing a very accurate description of the fidelity decay over the whole process. In this section, we study the accuracy of the linear response expression for the reduced dynamics of the qubit in the RMT model, as described in Sec. III B. The present situation is more complicated than in Ref. [27], since there are now two independent parameters which determine the dynamics, the coupling strength μ and the level splitting Δ. In addition, the object of interest is a two by two density matrix, not just a single function. In spite of these complications, we have seen that the ELR may be surprisingly accurate, as for instance in the case of Fig. 1 and Fig. 2.

For definiteness, we restrict ourselves to the case of eigenstates of σ_y as initial states. This has the advantage that the qubit state always tends to the maximally mixed state in the limit of large times. Thus, it is not necessary to introduce an additional fit parameter as in Eq. (46). Note that in Sec. IV D, following below, we show that eigenstates of σ_x as initial states in general lead to stationary states which are not maximally mixed.

In order to quantify the accuracy of the ELR we need to quantify the similarity between two states as they evolve in time, the first being obtained from numerical simulation $\varrho_{\rm c}^{\rm ns}(t)$ and the second from the ELR, $\varrho_{\rm c}^{\rm ELR}(t)$. For that purpose, we use the trace distance [37, 38], defined as

$$D[\varrho_{\rm c}^{\rm ns}(t),\varrho_{\rm c}^{\rm ELR}(t)] = {\rm tr}|\varrho_{\rm c}^{\rm ns}(t)-\varrho_{\rm c}^{\rm ELR}(t)|\,, \qquad (47)$$

where the absolute value $|A|$ of an operator A stands for $|A|=\sqrt{A^\dagger A}$. For a Hermitian matrix A, the trace of $|A|$ can be calculated conveniently as the sum of absolute values of the eigenvalues of A. For a two level system, it is straight forward to verify that the trace distance between two quantum states is proportional to their Euclidean distance in the Bloch sphere representation. Finally, in order to obtain a single number characterizing the similarity between two evolutions, we choose the maximum value of the distance in Eq. (47), taken over the full time range. This quantity is considered as a function of the parameters Δ and μ,

$$\mathcal{D}_{\rm max}(\Delta,\mu) = \max_t D[\varrho_{\rm c}^{\rm ns}(t),\varrho_{\rm c}^{\rm ELR}(t)]\,. \qquad (48)$$

In Fig. 5 we illustrate the application of our distance measure to two test cases, with $\Delta=1$ (red solid line) and $\Delta=1.5$ (blue dotted line), while $\mu=0.25$ in both cases. This is the only figure, where we increase the dimension of the environment to $N_{\rm e}=300$, in order to suppress residual finite size effects at very small times. It can be seen that the distance between the ELR approximation and the numerical simulation is varying strongly over time, with a general tendency to diminish towards larger times, where the qubit state approaches the completely mixed state. The quantity $\mathcal{D}_{\rm max}$ defined in Eq. (48) will select the global maximum value of each curve. The inset of Fig. 5 shows the modulus squared of the non-diagonal element of the average qubit state. There, we compare ELR approximations and numerical simulations on an absolute scale.

In Fig. 6, we quantify the accuracy of the ELR result

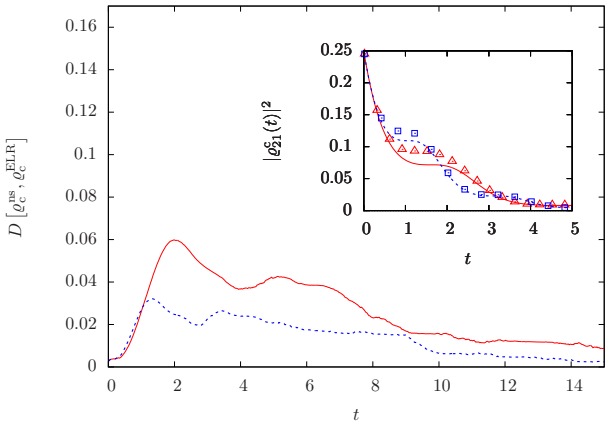

FIG. 5. (Color online) Trace distance between $\varrho_{\rm c}^{\rm ns}(t)$ and $\varrho_{\rm c}^{\rm ELR}(t)$, for the initial state being the symmetric eigenstate of σ_y and $\mu=0.25$. Red solid line corresponds to $\Delta=1$ and the blue dotted line to $\Delta=1.5$. The inset shows the modulus squared of the average non-diagonal matrix element of the qubit state. There, the red triangles (blue squares) and the red solid line (blue dotted line) correspond to the numerical simulation and the ELR, respectively.

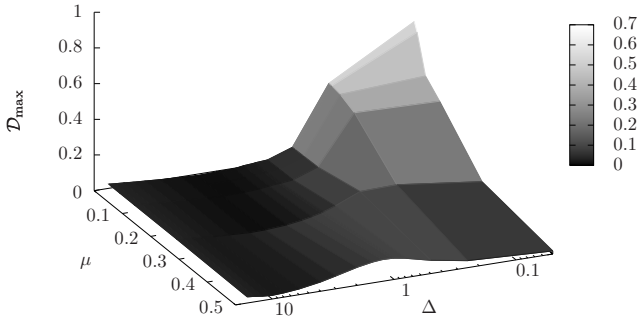

FIG. 6. Maximum trace distance between ELR approximation and numerical simulations as a function of the coupling strength μ and the energy splitting Δ, for the initial state being an eigenstate of σ_y.

as a uniform approximation over the whole decoherence process. For that purpose, we present a surface plot of $\mathcal{D}_{\max}(\Delta,\mu)$, based on 102 different points in the parameter space of μ and Δ. We can roughly distinguish two regions, one, where the ELR approximation works reasonably well, and one where it fails. The latter region can be located in the rectangle $0<\mu<0.3$ and $0<\Delta<0.8$, while everywhere else $D_{\max}$ is at least smaller than 0.2. Going away from that rectangular region, either by increasing Δ (keeping μ fixed), or by increasing μ (keeping Δ fixed), always results in the reduction of $D_{\max}$ to very small values. The slowest decay of the error can be observed for increasing μ at $\Delta\approx 1$. However, also there $D_{\max}$ becomes ever smaller when μ is further increased as we checked with additional simulations.

We may explain the success of the ELR approximation in the different limits as follows: For fixed Δ, when μ is increased, we arrive at the Fermi golden rule regime, where the ELR approximation becomes exact. For fixed μ, where Δ is increased, the double commutator in Eq. (16) has the function $\cos(\Delta s')$ as a common prefactor, see Eq. (33), such that the fast oscillations tend to suppress the s'-integral except for that part of the correlation function $c(s-s')$ which contains de δ-function. In this way we arrive again at the Fermi golden rule result. The fact that the ELR approximation fails in the limit of small Δ (for $\mu\lesssim 0.3$) and small μ (for $\Delta\lesssim 1$) suggests, that the ELR approximation is not consistent with a treatment on the basis of time-independent perturbation theory.

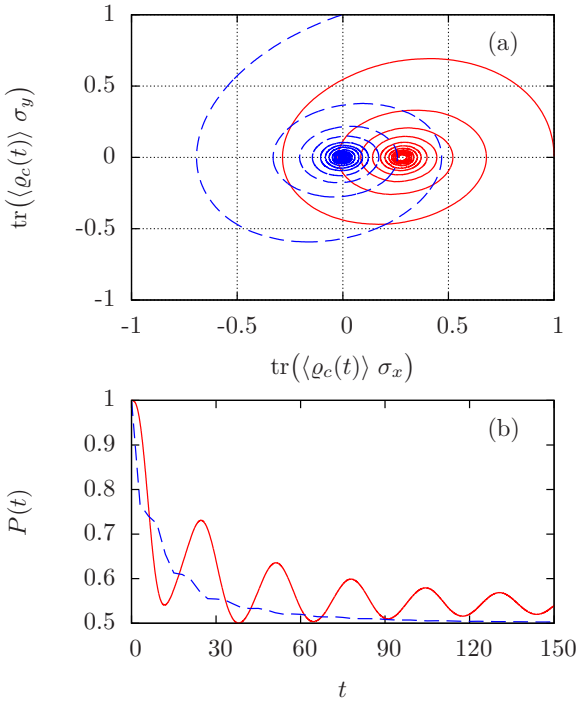

FIG. 7. (Color online) Decoherence process for $\Delta=0.25$ and $\mu=0.1$ for the initial state being an eigenstate of σ_x (red solid curves) and of σ_y (blue dashed curves). Panel (a): The trajectory of the average qubit state $\langle\varrho_{\rm c}(t)\rangle$ remains in the xy plane of the Bloch sphere. Panel (b): Purity as a function of time for the same cases.

D. Symmetry breaking stationary state

In this section, we investigate the stationary states of our model, $\langle\varrho_{\rm c}(t)\rangle$ in the limit $t\to\infty$. For some choices of the parameters Δ and μ, the system ends up in different stationary states, depending on the initial state. In other words, the system may remain in a given state (if so, this state would be called stationary) or not depending on the history of the evolution. This is very clearly a memory effect and a signature for non-Markovianity [39]. For the following discussion, the representation of the qubit states $\langle\varrho_{\rm c}(t)\rangle$ as points in the Bloch sphere will again prove useful.

Since the system Hamiltonian is proportional to σ_z, any qubit state at a finite distance of the z-axis will experience a torque, which can be computed from the Ehrenfest theorem. In the absence of any counteracting force, such a state will start to rotate around the z-axis. Therefore, one would expect that any stationary state must be located on the z-axis itself. Our numerical simulations show that this is not always the case. There are situations, where the coupling to the RMT environment breaks the rotational symmetry of the stationary state, which then settles on the x-axis at a finite distance from the origin.

For any state, starting out in the yz-plane of the Bloch sphere, the average qubit state $\langle\varrho_{\rm c}(t)\rangle$ will finally end up on the z-axis. As one can see from Fig. 3, starting out from an eigenstate of σ_z (this corresponds to either the South ($z=-1$) or the North pole ($z=1$) on the Bloch sphere, the evolution of the qubit state is always restricted to the z-axis, and the stationary state will typically be found at a finite distance from the origin, which represents the uniformly mixed state. By contrast, starting out on the y-axis, the evolution of $\langle\varrho_{\rm c}(t)\rangle$ is restricted to the xy-plane and the stationary state is precisely the uniformly mixed state, cf. Fig. 2. Because of the linearity of the mapping $\varrho_{\rm c}\to\langle\varrho_{\rm c}(t)\rangle$, any state in the yz-plane will be mapped on the z-axis as t goes to infinity.

It came as a surprise that in the case of a σ_x eigenstate as initial state, it is possible that $\langle\varrho_{\rm c}(t)\rangle$ converges to a state on the x-axis at a finite distance from the origin. This distance depends on the parameters Δ and μ and might be very small, as for instance in Fig. 1. However, choosing these parameters appropriately, the distance can be quite notable, as in Fig. 7, panel (a). In Fig. 7 we analyse the trajectory of the qubit state $\langle\varrho_{\rm c}(t)\rangle$ in the Bloch sphere, for $\Delta=0.25$ and $\mu=0.1$, for an eigenstate of σ_x (red solid line) and an eigenstate of σ_y (blue dashed line) as initial state. Both trajectories are restricted to the xy-plane ($z=0$), however, while the blue dashed line converges to the origin of the plane, i.e.

the completely mixed state, the red solid line clearly converges to a point on the x-axis approximately 0.3 units away from the origin. In panel (b), we show the purity of the corresponding two states. While the blue dashed line decreases with very small undulations towards the limit value $P(t) \to 1/2$, the red solid line shows strong oscillations, and seems to setlle on a value around $P(t) \to 0.55$. Note however, that the convergence is extremely slow.

As explained above, the only possibility for such a state to be a stationary state consists in the cancellation of the torque applied by the central system Hamiltonian due to the coupling term. Note however that σ_x cannot produce this compensation directly, as can be deduced by applying the Ehrenfest theorem, again. Instead, the compensating force must be exerted via the environment part of the state during the unitary dynamics in the full system (qubit plus environment). This is somewhat unexpected, because the environment part of the coupling operator is on average unitarily invariant, yet the individual terms in the ensemble are not.

Finally, note that Fig. 7 illustrates again the non-Markovianity of the evolution of the qubit. As we can see, the two different initial conditions lead to trajectories (the blue and the red line in upper panel) which intersect very often, but finally approach different equilibrium states. It is not shown here, but it is not difficult to find cases where the intersection happens exactly at the same time. In such a case, the evolution continues in different directions, even though the state is the same. Thus the continuation also depends on where the trajectory did come from – a clear manifestation of a memory effect.

V. CONCLUSIONS

Previous random matrix models for the environment and its coupling to the central system, e.g. [5, 6], assumed the lack of any knowledge about the coupling between central system and environments, thus yielding a generic result, equivalent to an average over different separable couplings. In this paper we identified different types of such couplings and derived an analytical description in the linear response approximation.

Concentrating on one particularly interesting case, we found a variety of rather unexpected features with a central system as simple as a single qubit. We developed an analytical description based on linear response theory, and investigated its accuracy. We described several effects in greater detail, such as purity oscillations, non-Markovian dynamics, and symmetry breaking stationary states. Some of these are clearly not of perturbative nature as we find them in numerics but not in our linear response solutions.

In future work we might consider different symmetry classes for the random matrix environment, as well as different couplings, e.g. similar to the Jaynes-Cummings coupling. Most importantly, we will try to improve the analytical description, e.g. incorporating time-independent perturbation theory. We also plan to study in more detail the degree of non-Markovianity, and the possibility to use time-local master equations for an accurate description of the dynamics of this open system.

ACKNOWLEDGMENTS

We thank C. Pineda and F. Toscano for enlightening discussions, and we acknowledge the hospitality of the Centro Internacional de Ciencias, UNAM, where many of these discussions took place. We also acknowledge financial support from CONACyT through the grants 129309 and 154586 as well as UNAM/DGAPA/PAPIIT IG 101113.

Appendix: Evaluation of integrals

In the present paper, we restrict the linear response calculations to the GUE case, where the basic correlation function reads:

$$c(t) = 1 + \delta(\tau) - b_2(\tau) \,, \qquad b_2(\tau) = \begin{cases} 1-\tau & : \tau < 1 \\ 0 & : \tau > 1 \end{cases} \,, \tag{A.1}$$

where $\tau = t/(2\pi)$ and we have assumed that $t > 0$. In this section we evaluate integrals which describe the evolution of the matrix elements of the density matrix of a qubit in contact with a random matrix environment in the interaction picture. The results are required in Sec. III.

1. Dephasing coupling $v_c = \sigma_z$

The evolution of the relevant quantity for this case, $\tilde{\varrho}_{21}(t)$, is given by the decay of a fidelity amplitude – see Eq. (23). We therefore denote the integral to be evaluated by $C_{\rm fid}(t)$. By changing the integration variable from s' to $u = s - s'$, we obtain:

$$\begin{aligned} C_{\rm fid}(t) &= \int_0^t {\rm d}s \int_0^s {\rm d}s'\; c(s-s') = \int_0^t {\rm d}u\; c(u)\; (t-u) = \frac{t^2}{2} + \pi\, t - \int_0^{\min(t,2\pi)} {\rm d}u\; \Big(1 - \frac{u}{2\pi}\Big)\,(t-u) \\ &= \frac{t^2}{2} + \pi\, t - \begin{cases} t^2/2 - t^3/(12\pi) & : t < 2\pi \\ \pi\, t - 2\pi^2/3 & : t > 2\pi \end{cases} = \begin{cases} \pi\, t + t^3/(12\pi) & : t < 2\pi \\ t^2/2 + 2\pi^2/3 & : t > 2\pi \end{cases} . \end{aligned} \tag{A.2}$$

2. Coupling operator $v_c = \sigma_x$

In this section, we evaluate the integrals required for the description of the non-commutative case, where the coupling operator is $\sigma_x \otimes V_{\rm e}$, which does not commute with the Hamiltonian of the central system.

a. The initial state of the central system being an eigenstate of σ_x

In order to calculate $C_x(t)$ in Eq. (31), we first calculate

$$b_x(u) = \int_u^t {\rm d}s\; {\rm e}^{-{\rm i}\Delta\, s}\; {\rm i}\; \sin\,\Delta(s-u) = \frac{1}{4\Delta}\Big[\,\big({\rm i} + 2\Delta\,(t-u)\big)\;{\rm e}^{-{\rm i}\Delta u} - {\rm i}\;{\rm e}^{{\rm i}\Delta\,(u-2t)}\,\Big] \tag{A.3}$$

and then divide the correlation function $c(u)$ in two parts, so that

$$C_x(t) = \bar{C}_x(t) - B_x(t)\;, \tag{A.4}$$

where

$$\begin{aligned} \bar{C}_x(t) &= \int_0^t {\rm d}u\; \big\{\,1 + \delta[u/(2\pi)]\,\big\}\; b_x(u) = \int_0^t {\rm d}u\; b_x(u) + \pi\; b_x(0) \\ B_x(t) &= \int_0^t {\rm d}u\; b_2(u)\; b_x(u) = \int_0^{\min(t,2\pi)} {\rm d}u\; \Big(1 - \frac{u}{2\pi}\Big)\; b_x(u)\;. \end{aligned} \tag{A.5}$$

This yields:

$$\bar{C}_x(t) = \frac{1}{4\Delta^2}\Big[\,4\,\big(1 - {\rm e}^{-{\rm i}\Delta\, t}\big) - (1 - {\rm i}\pi\Delta)\,\big(1 - {\rm e}^{-2{\rm i}\Delta\, t}\big) - 2\Delta\, t\,({\rm i} - \pi\Delta)\Big], \tag{A.6}$$

the integral over the two-point form factor yields:

$$\begin{aligned} B_x(t) = \frac{1}{4\pi\Delta^3}\Bigg[&(1 - 2\pi{\rm i}\Delta)\;\Delta\, t + 3\pi\,\Delta + \frac{5\,{\rm i}}{2} + \Big(\pi\Delta - \frac{\rm i}{2}\Big)\;{\rm e}^{-2{\rm i}\Delta\, t} \\ &+ \begin{cases} \big[\,2\Delta\,(t - 2\pi) - 2{\rm i}\,\big]\;{\rm e}^{-{\rm i}\Delta t} & : t < 2\pi \\ \Big[\,\Delta\,(2\pi - t) - \dfrac{5{\rm i}}{2}\,\Big]\;{\rm e}^{-2\pi{\rm i}\,\Delta} + \dfrac{\rm i}{2}\;{\rm e}^{2{\rm i}\Delta(\pi - t)} & : t > 2\pi \end{cases} \Bigg]\;. \end{aligned} \tag{A.7}$$

b. The initial state of the central system being an eigenstate of σ_y

Similar to the procedure in the case of the σ_x coupling, we first calculate

$$b_y(u) = \int_u^t {\rm d}s\; {\rm e}^{-{\rm i}\Delta\, s}\;\cos\,\Delta(s-u) = \frac{1}{4\Delta}\Big\{\,[2\Delta\,(t-u) - {\rm i}]\;{\rm e}^{-{\rm i}\Delta\, u} + {\rm i}\;{\rm e}^{{\rm i}\Delta\,(u-2t)}\,\Big\}\;. \tag{A.8}$$

Dividing the correlation function $c(u)$ in two parts,

$$C_y(t) = \bar{C}_y(t) - B_y(t) \ , \tag{A.9}$$

where

$$\bar{C}_y(t) = \int_0^t \mathrm{d}u \, \left\{ \, 1 - \delta[u/(2\pi)] \, \right\} \, b_y(u) = \int_0^t \mathrm{d}u \, b_y(u) + \pi \, b_y(0)$$

and

$$B_y(t) = \int_0^t \mathrm{d}u \, b_2(u) \, b_y(u) = \int_0^{\min(t,2\pi)} \mathrm{d}u \, \left(1 - \frac{u}{2\pi} \right) \, b_y(u) \ . \tag{A.10}$$

The evaluation of these integrals yield:

$$\bar{C}_y(t) = \frac{1}{4\Delta^2} \Big[\, 2\Delta \, t \, (\pi\Delta - \mathrm{i}) + (1 - \mathrm{i}\pi\Delta) \, \left(1 - \mathrm{e}^{-2\mathrm{i}\Delta \, t} \right) \Big] \ , \tag{A.11}$$

and

$$B_y(t) = \frac{1}{4\pi\Delta^3} \left[(1 - 2\pi\mathrm{i} \, \Delta) \, \Delta \, t + \pi\Delta + \frac{3\mathrm{i}}{2} + \left(\frac{\mathrm{i}}{2} - \pi\Delta \right) \, \mathrm{e}^{-2\mathrm{i}\Delta \, t} \begin{cases} 2\mathrm{i} \, \mathrm{e}^{-\mathrm{i}\Delta \, t} & : t < 2\pi \\ \dfrac{\mathrm{i}}{2} \, \mathrm{e}^{2\mathrm{i}\Delta(\pi - t)} + \left[\dfrac{3\mathrm{i}}{2} - (2\pi - t) \, \Delta \right] \, \mathrm{e}^{-2\pi\mathrm{i}\Delta} & : t > 2\pi \end{cases} \right] \ . \tag{A.12}$$

c. The initial state of the central system being an eigenstate of $\boldsymbol{\sigma_z}$

In this case

$$C_z(t) = \int_0^t \mathrm{d}s \, \int_0^s \mathrm{d}u \, c(u) \, \cos(\Delta u) = \int_0^t \mathrm{d}u \, c(u) \, \cos(\Delta u) \, (t - u) \ . \tag{A.13}$$

Separating the integral in the same way as above, we find

$$C_z(t) = \bar{C}_z(t) - B_z(t) \ , \quad \text{where} \quad \bar{C}_z(t) = \frac{1 - \cos \, \Delta t}{\Delta^2} + \pi \, t \tag{A.14}$$

and

$$B_z(t) = \int_0^{\min(t,2\pi)} \mathrm{d}u \, \left(1 - \frac{u}{2\pi} \right) \, \cos(\Delta u) \, (t - u), \tag{A.15}$$

evaluating the above integral we obtain finally:

$$B_z(t) = \frac{1}{\Delta^2} \left[1 + \frac{t}{2\pi} - \begin{cases} \frac{\sin \, \Delta t}{\pi\Delta} + \left(1 - \dfrac{t}{2\pi} \right) \, \cos \, \Delta t & : t < 2\pi \\ \frac{\sin \, 2\pi\Delta}{\pi\Delta} - \left(1 - \dfrac{t}{2\pi} \right) \, \cos \, 2\pi\Delta & : t > 2\pi \end{cases} \right] \ . \tag{A.16}$$

[1] E. Lutz and H. A. Weidenmüller, Physica A **267**, 354 (1999)

[2] T. Gorin and T. H. Seligman, J. Opt. B: Quant. Semiclass. Opt. **4**, S386 (2002)

[3] T. Gorin and T. H. Seligman, Phys. Lett. A **309**, 61 (2003)

[4] M. Žnidarič, C. Pineda, and I. García-Mata, Phys. Rev. Lett. **107**, 080404 (2011)
[5] C. Pineda, T. Gorin, and T. H. Seligman, New J. Phys. **9**, 106 (2007)
[6] T. Gorin, C. Pineda, H. Kohler, and T. H. Seligman, New J. Phys. **10**, 115016 (2008)
[7] Vinayak and M. Žnidarič, J. Phys. A: Math. Theor. **45** (2012)
[8] J. Novotný, G. Alber, and I. Jex, J. Phys. A: Math. Theor. **42**, 282003 (2009)
[9] J. Novotný, G. Alber, and I. Jex, New J. Phys. **13**, 053052 (2011)
[10] W. Bruzda, V. Cappellini, H.-J. Sommers, and K. Życzkowski, Phys. Lett. A **373**, 320 (2009)
[11] M. Musz, M. Kuś, and K. Życzkowski, Phys. Rev. A **87**, 022111 (2013)
[12] J. Wang, J. Opt. Soc. Am. B **29**, 75 (2012)
[13] S. A. Gardiner, J. I. Cirac, and P. Zoller, Phys. Rev. Lett. **79**, 4790 (1997)
[14] T. Gorin, T. Prosen, T. H. Seligman, and W. T. Strunz, Phys. Rev. A **70**, 042105 (2004)
[15] H. J. Kimble and L. Mandel, Phys. Rev. A **13**, 2123 (1976)
[16] E. T. Jaynes and F. W. Cummings, Proc. IEEE **51**, 89 (1963)
[17] E. P. Wigner, SIAM Rev. **9**, 1 (1967)
[18] R. Balian, Nuovo Cimento **57B**, 183 (1967)
[19] G. Casati, F. Valz-Gris, and I. Guarneri, Lett. Nuovo Cimento **28**, 279 (1980)
[20] O. Bohigas, M. J. Giannoni, and C. Schmit, Phys. Rev. Lett. **52**, 1 (1984)
[21] G. B. Lemos, R. M. Gomes, S. P. Walborn, P. H. Souto Ribeiro, and F. Toscano, Nat. Commun. **3**, 1211 (2012)
[22] M. V. Berry and M. Tabor, Proc. R. Soc. Lond. A **356**, 375 (1977)
[23] I. Bengtsson and K. Życzkowski, *Geometry of Quantum States: An Introduction to Quantum Entanglement* (Cambridge University Press, Cambridge, 2006)
[24] H.-P. Breuer, E.-M. Laine, and J. Piilo, Phys. Rev. Lett. **103**, 210401 (2009)
[25] A. Rivas, S. F. Huelga, and M. B. Plenio, Phys. Rev. Lett. **105**, 050403 (2010)
[26] M. L. Mehta, *Random Matrices and the Statistical Theory of Energy Levels, 3rd Ed.* (Academic Press, New York, 2004)
[27] T. Gorin, T. Prosen, and T. H. Seligman, New J. Phys. **6**, 20 (2004)
[28] H.-J. Stöckmann and R. Schäfer, New J. Phys. **6**, 199 (2004)
[29] H.-J. Stöckmann and R. Schäfer, Phys. Rev. Lett. **94**, 244101 (2005)
[30] T. A. Brody, J. Flores, J. B. French, P. A. Mello, A. Pandey, and S. S. M. Wong, Rev. Mod. Phys. **53**, 385 (1981)
[31] T. Gorin, T. Prosen, T. H. Seligman, and M. Žnidarič, Phys. Rep. **435**, 33 (2006)
[32] F. Haake, *Quantum Signatures of Chaos, 2nd Ed.* (Springer, Berlin, 2001)
[33] T. Prosen, Phys. Rev. E **65**, 036208 (2002)
[34] T. Prosen and M. Žnidarič, J. Phys. A: Math. Gen. **35**, 1455 (2002)
[35] T. Gorin, F.-M. Dittes, M. Müller, I. Rotter and T. H. Seligman, Phys. Rev. E **56**, 2481 (1997)
[36] T. Gorin, J. Phys. A: Math. Gen. **32**, 2315 (1999)
[37] C. A. Fuchs and J. van de Graaf, arXiv: quant-ph/9712042 (1997)
[38] A. Gilchrist, N. K. Langford, and M. A. Nielsen, Phys. Rev. A **71**, 062310 (2005)
[39] H.-P. Breuer, and F. Petruccione, *The Theory of Open Quantum Systems* (Oxford University Press, Oxford, 2002)